Available online at www.sciencedirect.com

SciVerse ScienceDirect

Ceramics International 38 (2012) 3947–3953

CERAMICS INTERNATIONAL

www.elsevier.com/locate/ceramint

Hard polycrystalline eutectic composite prepared by spark plasma sintering

I. Bogomol [a,b,c,*], S. Grasso [d], T. Nishimura [b], Y. Sakka [b], P. Loboda [a], O. Vasylkiv [b,c]

[a] National Technical University of Ukraine "KPI", Peremogy av. 37, Kyiv 03056, Ukraine
[b] National Institute for Materials Science, 1-2-1, Sengen, Tsukuba, Ibaraki 305-0047, Japan
[c] Nanyang Technological University, 50 Nanyang Avenue, 639798 Singapore, Singapore
[d] Nanoforce Technology Ltd and School of Engineering and Materials Science, Queen Mary University of London, London E1 4NS, UK

Received 4 January 2012; accepted 16 January 2012
Available online 25 January 2012

Abstract

A polycrystalline eutectic B_4C–TiB_2 composite was prepared by spark plasma sintering. The starting eutectic powder was obtained by mechanical grinding of the directionally solidified eutectic B_4C–TiB_2 alloy. The microstructure of the polycrystalline composite exhibited randomly oriented eutectic grains with an average size of about 50–100 μm. Eutectic grains consisted of boron carbide matrix reinforced by titanium diboride inclusions. The secondary eutectic structure in the grain boundary is formed at sintering temperature higher than 1700 °C. XRD analysis revealed that the eutectic B_4C–TiB_2 composite consist mainly of B_4C and TiB_2 phases. The measured Vickers hardness was in the range of 32.35–54.18 GPa and the average fracture toughness of the samples was as high as 4.81 MPa $m^{1/2}$. The bending strengths of the composite evaluated at room temperature and at 1600 °C were 230 and 190 MPa, respectively.

Keywords: B. Composites; C. Hardness; D. Borides; Spark plasma sintering

1. Introduction

Due to their unique combination physical and mechanical properties, boron carbide based materials are increasingly used in several industrial sectors. The boron carbide crystal structure B_4C exhibits strong covalent bonding, which results in high hardness, augmented Young's modulus and elevated melting point [1]. Furthermore, boron carbide shows low density (2.53 g/cm^3). The boron carbide is semiconductor, however the presence of small amounts of metal impurities can affect significantly the electrical conductivity. The excellent strength-to-weight ratio makes boron carbide attractive materials to be employed in various fields such as tooling, high-temperature structural materials and thermoelectrics [2]. If compared to traditional refractory metals, such as W, Mo, Ta and Nb [3,4], the application fields of boron carbide ceramics are limited by its low fracture toughness.

Due to its brittleness, monolithic B_4C is not used as structural material. The B_4C toughness is enhanced by using various metallic additives as well as high-energy compacting methods [5]. The fibres reinforcement, realized by directional solidification of quasibinary eutectics of systems B_4C–RC (where RC – refractory compounds – TiB_2, ZrB_2, HfB_2, SiC, etc.) [6–10] represents one of the most effective method to enhance the fracture toughness. At present the directional solidification allows to obtain ceramic materials with strength above 4.5 GPa. Such high value is attributable to the highly oriented structure, elongated grains, good bonding between the phases and defect free crystals [11–13]. Unfortunately the directional solidification method results in limited size products (i.e. sample diameter 8 mm) and strong anisotropy of the mechanical properties due to the marked texturing of the grains.

Spark plasma sintering (SPS) is a rapid sintering technique which was recently developed for the rapid fabrication of dense ceramics and composites at low sintering temperatures compared to the conventional sintering methods as hot pressing (HP). Both SPS and HP are pressure assisted sintering method, an uniaxial pressure is applied across the specimen during the sintering process. However, SPS and HP differ significantly in the heating mode. Specifically, in HP an array of heating

* Corresponding author at: National Technical University of Ukraine "KPI", Peremogy av. 37, Kyiv 03056, Ukraine. Tel.: +380 44 406 82 15; fax: +380 44 406 82 15.
E-mail address: ubohomol@iff.kpi.ua (I. Bogomol).

0272-8842/$36.00
doi:10.1016/j.ceramint.2012.01.048

elements indirectly heats the punch/powder/die assembly by radiation and eventually by convection and/or conduction. The powder heating rate is controlled by the rate of radiation and/or convection and conduction. Conversely, in SPS, the punches transfer the pulsed current (typically a thousand amperes) and Joule heat directly to the powder. In the SPS, the current effects are not limited to Joule heating, thus other non-thermal effects as current enhanced mass transport, electroplasticity, and reactivity [14–18] have been identified. The applied pressure, in turn, indirectly aids in the densification process by increasing the surface energy driving force. Even if there is no direct evidence existence of plasma [19] during the sintering, the SPS has the well recognized ability to produce fully dense material which cannot be obtained by conventional sintering methods. The SPS permits to avoid grain coarsening whilst promoting densification due to the short heating and the cooling times [20–22].

In the present work, the SPS densification mechanisms of eutectic powder were investigated aiming to obtain an isotropic fibre reinforced B_4C–TiB_2 ceramic. As reported in Refs. [23,24], the pseudo-binary systems of borides produced by zone melting resulted in improved microhardness and fracture toughness if compared to the monophasic compositions (i.e. B_4C or TiB_2). The fracture mode of brittle polycrystalline materials at near room temperatures is dominated by transcrystalline mechanism [25], thus, randomly oriented eutectic particles consisting of boron carbide directionally reinforced by titanium diboride might contribute to increase the toughness of the isotropic ceramic material.

2. Experimental details

The eutectic powder with average grain size 50–100 μm was obtained by mechanical grinding of the directionally solidified eutectic B_4C–TiB_2 alloy in a steel mortar. The directionally solidified eutectic B_4C–TiB_2 composite was produced by a floating zone method based on crucibleless zone melting of the compacted powders as described in Ref. [26]. B_4C–TiB_2 particle size smaller than 50–100 μm is undesired, it results in the destruction of regular eutectic microstructure within the individual particles.

As shown in Fig. 1 the eutectic consists of 77 vol% of boron carbide matrix and 23 vol% of titanium diboride inclusions. The average TiB_2 inclusion diameter and interphase spacing are 0.5–1 and 1–1.5 μm, respectively. In order to remove the wear products of steel mortar, a magnetic separation was employed. The typical X-ray diffraction pattern of the B_4C–TiB_2 powder after magnetic separation is shown in Fig. 2(a). XRD analysis revealed that composite consisted of B_4C and TiB_2 phases. No other phase was identified.

Spark plasma sintering was carried out in an SPS apparatus (SPS-1050, SPS Syntex Inc., Japan) using a graphite die with an inner diameter of 10 and 20 mm. The temperature was controlled by an optical pyrometer focused on the non-through hole located on the surface of the graphite die. The sintering experiments were conducted in vacuum (1.3×10^{-3} Pa) atmosphere at different temperatures in the range of 1400–1900 °C and dwelling time of 1–20 min under a pressure of 50–100 MPa. The heating and

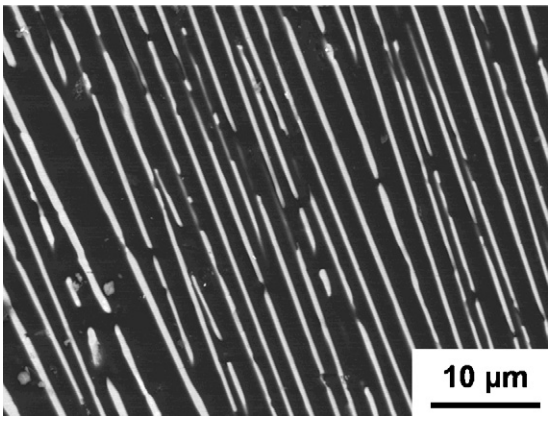

Fig. 1. Microstructure of the directionally solidified eutectic B_4C–TiB_2 alloy.

cooling rates were 100 °C/min. In order to decrease the radial temperature gradient inside the punch-sample-die assembly, an insulating felt was used. For easy sample extraction after sintering, a graphite paper was inserted between the powder and the die/punch. The sintered samples had diameter 10 and 20 mm. Densities and porosity of all sintered samples were measured using the Archimedes method with distilled water as the immersion medium.

The Vickers hardness and fracture toughness were measured using a standard indentation technique. Prior to indentation, the samples were polished with diamond abrasives to a 3-μm finish. Hardness tests (PMT-3, Russia) were performed at a load of 2 N and a holding time of 15 s. The fracture toughness, K_{IC}, was determined directly from the crack lengths produced by Vickers indentations (PMT-3, Russia) at 2 N load with a 15 s dwell time.

The fracture toughness values were calculated using Eq. (1) given by Niihara et al. [27] for the Palmqvist cracks in brittle materials:

$$K_{IC} = 9.052 \times 10^{-3} H^{3/5} E^{2/5} dl^{-1/2} \quad (1)$$

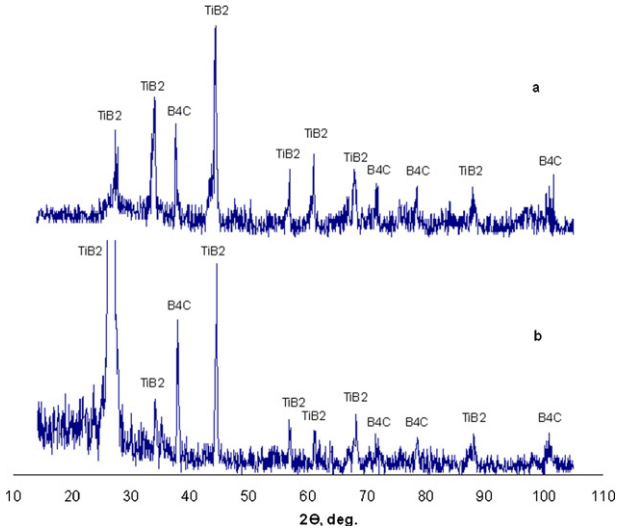

Fig. 2. X-ray diffraction patterns of the eutectic B_4C–TiB_2 powder (a) and sintered sample at 1800 °C for 20 min (b).

where H is the Vickers hardness, E is Young's modulus, d is the average diagonal line length of the indentation and l is the average length of the cracks. For each sample, nine indentations were made to obtain the average hardness and crack lengths to compute fracture toughness.

For analysis, the sintered samples with diameter of 20 mm were cut into rectangular 2.5 mm × 3 mm × 20 mm blocks by an electric discharge machining. Their lateral surfaces were grounded and polished using diamond pastes. Microstructural investigations of the spark plasma sintered B_4C–TiB_2 composites and fracture surfaces were performed by means of scanning electron microscopy (JEOL JSM-7001F, Tokyo, Japan). Phase identification was performed by X-ray diffractometry (XRD: DRON-3M, Russia) with CuK_a radiation. The three-point bending strength tests were conducted at room temperature and at 1600 °C, in vacuum 1.3×10^{-3} Pa, using an ''Instron 4505'' setup (UK). The specimens of 3 mm × 2.5 mm × 20 mm were placed into graphite containers on the SiC supports spaced by 16 mm. The graphite containers were chambered on the turret of the testing machine. After vacuumization specimens were feeded into heating area for bending strength test operation. The loading speed was 0.5 mm/min. Four to six samples were tested at each temperature and the measurement accuracy was taken as the standard deviation.

3. Results and discussion

3.1. Microstructure

In order to optimize the sintering conditions of the eutectic powders and hence the properties of the sintered B_4C–TiB_2 ceramic, SPS was conducted in the range of 1400–1900 °C with dwell times from 1 to 20 min.

SEM micrographs of the spark plasma sintered B_4C–TiB_2 samples are shown in Fig. 3. The polycrystalline composite consists of randomly oriented eutectic grains. Each eutectic grain is characterized by dark gray boron carbide matrix reinforced by light colour titanium diboride inclusions. The average TiB_2 inclusion diameter and interphase of 0.5–1 and 1–1.5 μm, respectively, corresponded to initial parameters before sintering. The average grain size of the sintered samples (about 50–100 μm) corresponded to starting size of the grinded eutectic particles.

The X-ray diffraction patterns of the spark plasma sintered at 1800 °C B_4C–TiB_2 sample is shown in Fig. 2(b). XRD analysis revealed that it consists mainly of B_4C and TiB_2 phases. No other phase was identified.

The microstructure of the grain boundaries is strongly affected by the sintering temperature and dwell times. B_4C–TiB_2 sample sintered at 1400–1500 °C shows dense eutectic

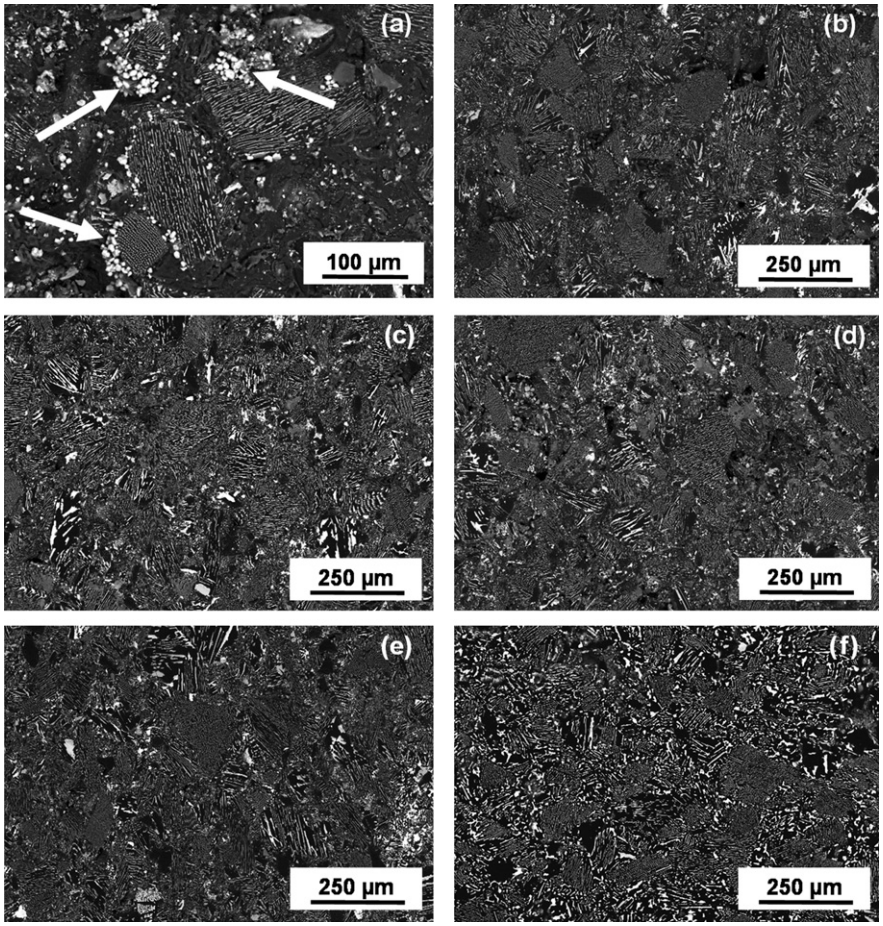

Fig. 3. Microstructure of the eutectic B_4C–TiB_2 composites sintered for 1 min at: (a) 1400 °C (arrows show the rounded TiB_2 particles), (b) 1500 °C, (c) 1600 °C, (d) 1700 °C, (e) 1800 °C, and (f) 1900 °C.

grains bonded to each with highly porous interconnection zone filled by small chips formed during grinding process (Fig. 4(a) and (b)). During the sample polishing, the intensive chipping of low temperature sintered samples indicated a relatively weak bond between the grains (Fig. 3). In the samples sintered at 1400–1500 °C, light colour rounded TiB_2 particles are observed (Fig. 3(a)). The rounded titanium diboride inclusions resulted from the initial grinding of the B_4C–TiB_2 eutectic composition. A further increasing of sintering temperature and dwell times promoted complete particles bonding. Thus, the rounded TiB_2 particles were not observed (Fig. 4).

The SEM micrograph (Fig. 4(b)) of the sample sintered at 1600 °C indicates that the diboride inclusions inter-grew in the neighbouring grains by forming strong intergranular bond (Fig. 4(b)), hereinafter defined as secondary eutectic structure. This is clearly observed for the samples sintered at 1800 °C with dwell times of 7–20 min, where the secondary eutectic structure is detected (Fig. 4(d)).

As shown in Fig. 4(e), the increasing of sintering temperature up to 1900 °C led to a degradation of the eutectic structure due to the coarsening of the diboride inclusions. Such grain coarsening is detrimental to the mechanical properties.

A shown in Fig. 5, the residual porosity of the SPSed B_4C–TiB_2 decreased by increasing the sintering temperature and dwell times. Density of 97–98% was achieved for the samples sintered at 1800 °C for 20 min or at 1900 °C for 1 min under a compaction pressure of 100 MPa. Regardless the dwell time, higher the temperature, higher the relative density. This phenomenon is apparently similar to the hot pressing and conventional pressureless sintering [20,28]. As shown in Fig. 5, the full densification is achievable at temperatures of at least 1800 °C. Such temperature should be associated with the creep plastic deformation in the eutectic B_4C–TiB_2 alloy (Fig. 5(a)). Significant plastic deformation of the eutectic grains is not observed in the microstructures of the samples below 1800 °C (Figs. 3 and 4).

The decreasing of porosity during SPS at temperatures higher 1800 °C (Fig. 5(b)) occurred due the microplastic deformation in the eutectic B_4C–TiB_2 grains, the planes of the easiest dislocation glide of the boron carbide matrix coincided with loading direction (Fig. 4(c)). The increasing of the dwell time from 1 to 20 min at 1800 °C significantly intensified the shrinkage and reduced the sample porosity (Fig. 5(b)) confirming the occurrence of time dependent thermally activated plastic deformation at this temperature. Thus the

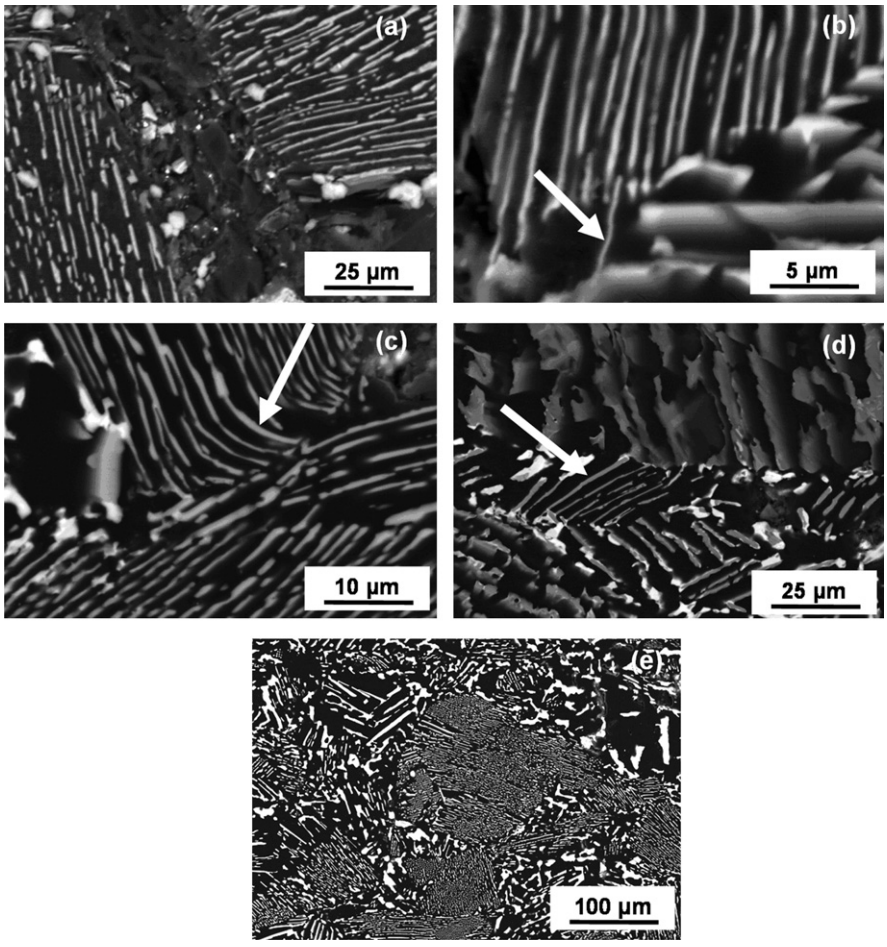

Fig. 4. Microstructure of the grain boundaries of the eutectic B_4C–TiB_2 composites sintered at: (a) 1400 °C for 1 min, (b) 1600 °C for 1 min (arrow shows the intergrowth of the diboride inclusion), (c) 1800 °C for 1 min (arrow shows the plastic deformation of the material), (d) 1800 °C for 7 min (arrow shows the secondary eutectic structure) and (e) 1900 °C for 1 min.

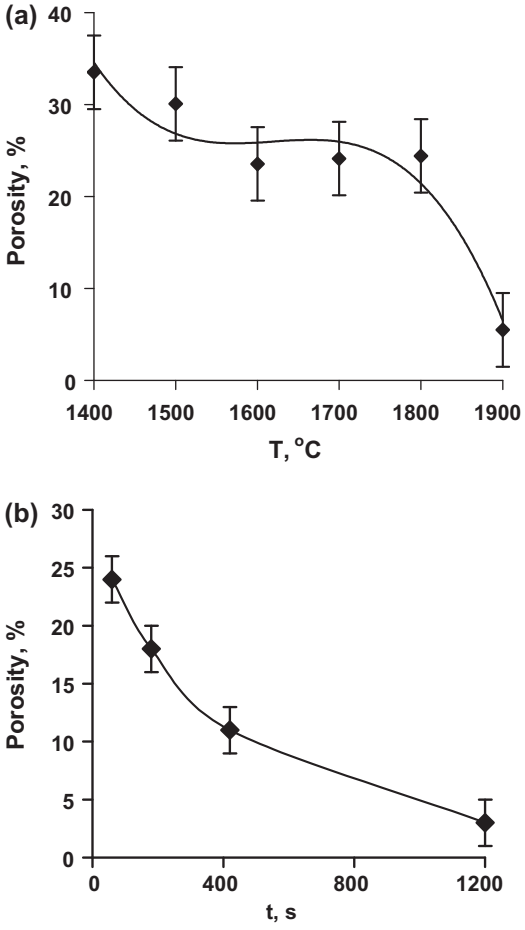

Fig. 5. Residual porosity dependence of the eutectic B_4C–TiB_2 composites as function of SPS temperature (a) and dwell time (b) of samples sintered at 1800 °C.

change from the brittle to ductile fracture mode for the spark plasma sintered B_4C–TiB_2 eutectic composite should be expected at temperatures above 1800 °C.

3.2. Vickers hardness

The hardness and fracture toughness of the ceramics consolidated by SPS are summarized in Table 1. The mechanical properties of the sintered ceramics at 1400–1500 °C are not presented in this study because of the low values, which were caused by the high residual porosity.

The measured Vickers hardness values are found to lie in the range of 32.35–54.18 GPa for the samples sintered by SPS at 1600–1900 °C for 1–20 min. The hardnesses measured in present study are higher than those obtained by other investigators (36 GPa [29], 31 GPa [30] and 41 GPa [31]). As seen, there is a no obvious correlation between the hardness and porosity. However for the samples sintered at 1800 °C there is an increasing in the hardness with dwell time/relative density (Fig. 5(b)). The hardness is affected by the microstructural features, such as grain size, orientation, porosity, and grain boundary constitution [32]. The highest average hardness of 54.18 GPa was demonstrated by the sample sintered at 1800 °C for 20 min with a relative density of 98.8%. The minimum average hardness of 32.35 GPa was achieved in the sample sintered at 1600 °C for 1 min mainly due the low relative density (77.1%). The low hardness about 41 GPa, for the samples sintered at 1900 °C was attributed to the significant grain coarsening (Figs. 3(f) and 4(e)).

3.3. Fracture toughness

The fracture toughness values, calculated from the crack lengths by applying the Niihara's equation [27], are shown in Table 1. The indentation toughness data revealed that the average fracture toughness of the samples consolidated by SPS at 1600–1900 °C for 1–20 min ranged between 1.78 and 4.81 MPa $m^{1/2}$.

Similar fracture toughness values were previously reported [4,29,31,33]. These values are slightly lower than fracture toughness of the directionally solidified B_4C–TiB_2 eutectic alloy [23]. The observations of the cracks nucleated from the corners of the Vickers indentations revealed that crack deflection and bridging toughening mechanisms contributed to improve the fracture toughness of the eutectic B_4C–TiB_2. It is well-known that the crack deflection in fibre-reinforced or laminated ceramics is achieved through weak fibre–matrix interfaces, or, as in the present investigation, through low toughness phase as B_4C in the composite [11].

3.4. Bending strength

For samples sintered at 1900 °C the bending strength tests were carried out at room temperature and at 1600 °C. It is

Table 1
Micromechanical properties of the spark plasma sintered samples.

SPS parameters		Vickers hardness, GPa	K_{IC}, MPa $m^{1/2}$	Relative density, %
Temperature, °C	*t*, min			
1600	1	32.35	1.78	76.46
1700	1	38.47	3.23	75.89
1800	1	44.31	3.87	75.58
1800	3	48.69	4.32	82.18
1800	7	53.43	4.66	89.57
1800	20	54.18	4.81	97.46
1900	1	42.31	4.01	94.51
1900	10	41.54	4.21	97.34
1900	20	41.86	4.15	98.18

shown that the strength of the spark plasma sintered B_4C–TiB_2 eutectic alloy at room temperature reaches 230 MPa which slightly exceeds the 190 MPa for the directionally solidified eutectic alloy of the same composition [7]. This result can be attributed (i) to the partial relaxation of residual microstresses given by the differential thermal expansion between boron carbide matrix and titanium diboride inclusions, and (ii) to the isotropy of microstructure on the mesolevel leading to material strengthening by the grain boundary mechanisms.

The investigation of the fracture surface of the samples shows that the composites tested at room temperature have predominantly mixed brittle fracture modes: transcrystalline and intercrystalline mechanisms (Fig. 6(a)). For samples tested at 1600 °C, mainly brittle intercrystalline mechanism of the fracture is observed (Fig. 6(b)). This effect indicates a sufficient grain boundaries weakening at 1600 °C. As a result the bending strength of the SPSed B_4C–TiB_2 eutectic alloy measured at 1600 °C was 180 MPa which is slightly lower than 230 MPa of the directionally solidified eutectic alloy [7]. It is well-known that at elevated temperatures polycrystalline materials are fractured mainly by intercrystalline mechanism [5]. The grain boundaries, which represent the outflows of various defects as pores, become the weak point to nucleate the fracture.

Waku et al. [34], on the base of high-resolution TEM investigation, reported that the grain boundaries of sintered composites contain amorphous phases. The existence of amorphous phases at interfaces or grain boundaries generally leads to a reduction in the strength of the material at high temperature [35,36]. Amorphous phases are observed at the grain boundary of the sintered composite, also at the triple-grain junctions and grain boundaries between eutectic phases in the sintered composite. On the contrary, in the directionally solidified eutectic composite, no amorphous phases are observed at the interfaces between eutectic phases and relatively congruent interfaces are formed [34]. Similarly, the perfection of grain boundaries and interfaces is a another component to enhance high-temperature strength. Thus directionally solidified eutectic alloys exhibits higher mechanical properties at elevated temperatures than sintered polycrystalline materials.

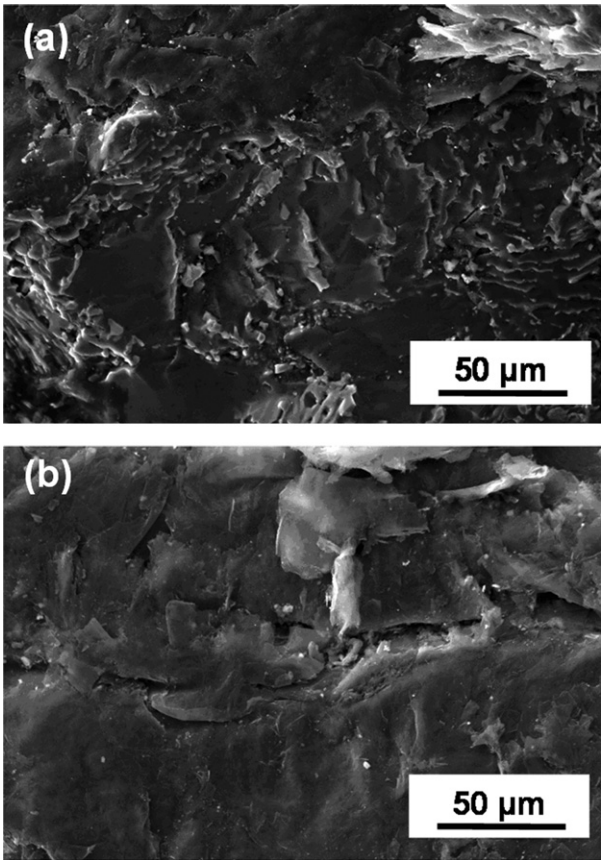

Fig. 6. Microstructure of the fracture surfaces of the eutectic B_4C–TiB_2 composites tested at room temperature (a) and at 1600 °C (b).

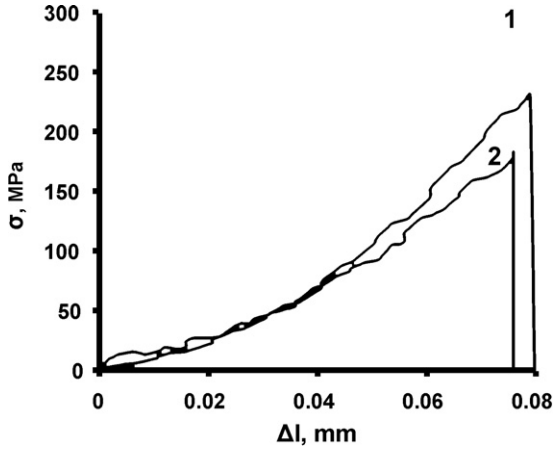

Fig. 7. Load–displacement curves of the sintered eutectic B_4C–TiB_2 samples tested at room temperature (1) and at 1600 °C (2).

The load–displacement curves for the spark plasma sintered B_4C–TiB_2 samples tested at room temperature and at 1600 °C (Fig. 7) correspond to the brittle fracture mode [27]. The curves are similar to directionally solidified B_4C–TiB_2. However for the samples tested at 1600 °C the curve slope, and accordingly Young's modulus, are significantly lower than the ones tested at room temperature. The presence of steps in the 1600 °C curve indicates the intercrystalline fracture mechanism of the samples (Fig. 7).

4. Conclusions

Polycrystalline eutectic B_4C–TiB_2 alloy was prepared by spark plasma sintering. The microstructure of the composite represents the polycrystalline material consisting of B_4C–TiB_2 eutectic grains randomly oriented in material. The secondary eutectic structure in grain boundary is formed at sintering temperature higher 1700 °C. The Vickers hardness of the samples was found to lie in the range of 32.35–54.18 GPa and fracture toughness as high as 4.81 MPa $m^{1/2}$. Investigation of mechanical properties showed that the room temperature bending strength of the SPSed B_4C–TiB_2 eutectic alloy showed higher strength than the directionally solidified. At elevated temperatures inverse behaviour of the strength was observed.

References

[1] V. Matkovich, Boron and Refractory Borides, Springer-Verlag, Berlin, 1977.

[2] T.J. Holmquist, G.R. Johnson, Response of boron carbide subjected to high-velocity impact, International Journal of Impact Engineering 35 (8) (2008) 742–752.

[3] V. Skorokhod, V. Krstic, Processing, microstructure, and mechanical properties of B_4C–TiB_2 particulate sintered composites: part I. Pressureless sintering and microstructure evolution, Powder Metallurgy and Metal Ceramics 39 (7–8) (2000) 414–423.

[4] V. Skorokhod, V. Krstic, Processing, microstructure, and mechanical properties of B_4C–TiB_2 particulate sintered composites: part II. Fracture and mechanical properties, Powder Metallurgy and Metal Ceramics 39 (9–10) (2000) 504–513.

[5] Narottam P. Bansal, Handbook of Ceramic Composites, Kluwer, Academic Publishers, Boston, 2005.

[6] R.L. Ashbrook, Directionally solidified ceramic eutectics, Journal of the American Ceramic Society 60 (9–10) (1977) 428–435.

[7] I. Bogomol, T. Nishimura, O. Vasylkiv, Y. Sakka, P. Loboda, Microstructure and high-temperature strength of B_4C–TiB_2 composite prepared by a cruciibleless zone melting method, Journal of Alloys and Compounds 485 (1–2) (2009) 677–681.

[8] J. Llorca, V.M. Orera, Directionally solidified eutectic ceramic oxides, Progress in Materials Science 51 (2006) 711–809.

[9] I. Bogomol, O. Vasylkiv, Y. Sakka, P. Loboda, Mechanism of nucleation and growth of directionally crystallized alloys of the B_4C–MeB_2 system, Journal of Alloys and Compounds 490 (1–2) (2010) 557–561.

[10] I. Bogomol, T. Nishimura, O. Vasylkiv, Y. Sakka, P. Loboda, High-temperature strength of directionally solidified B_4C–ZrB_2 composite, World Journal of Engineering 7 (2) (2010) 314–320.

[11] P.B. Oliete, J.I. Pena, A. Larrea, V.M. Orera, J. Llorca, J.Y. Pastor, A. Martin, J. Segurado, Ultra-high-strength nanofibrillar Al_2O_3–YAG–YSZ eutectics, Advanced Materials 19 (2007) 2313–2318.

[12] I. Bogomol, T. Nishimura, O. Vasylkiv, Y. Sakka, P. Loboda, High-temperature strength of directionally reinforced LaB_6–TiB_2 composite, Journal of Alloys and Compounds 505 (1) (2010) 130–134.

[13] I. Bogomol, T. Nishimura, Yu. Nesterenko, O. Vasylkiv, Y. Sakka, P. Loboda, The bending strength temperature dependence of the directionally solidified eutectic LaB_6–ZrB_2 composite, Journal of Alloys and Compounds 509 (20) (2011) 6123–6129.

[14] R. Chaim, O. Reinharz Bar-Hama, Densification of nanocrystalline NiO ceramics by spark plasma sintering, Materials Science and Engineering: A 527 (3) (2010) 462–468.

[15] W. Chen, U. Anselmi-Tamburini, J.E. Garay, J.R. Groza, Z.A. Munir, Fundamental investigations on the spark plasma sintering/synthesis process: I. Effect of dc pulsing on reactivity, Materials Science and Engineering: A 394 (1–2) (2005) 132–138.

[16] U. Anselmi-Tamburini, J.E. Garay, Z.A. Munir, A. Tacca, F.G. Maglia, Spinolo Spark plasma sintering and characterization of bulk nanostructured fully stabilized zirconia: part I. Densification studies, Journal of Materials Research 19 (2004) 3255–3262.

[17] G. Bernard-Granger, C. Guizard, Spark plasma sintering of a commercially available granulated zirconia powder: I. Sintering path and hypotheses about the mechanism(s) controlling densification, Acta Materialia 55 (10) (2007) 3493–3504.

[18] S. Grasso, Y. Sakka, G. Maizza, Electric current activated/assisted sintering (ECAS): a review of patents 1906–2008, Science and Technology of Advanced Materials 10 (2009), 053001.

[19] D.M. Hulbert, A. Anders, J. Andersson, E.J. Lavernia, A.K. Mukherjee, A discussion on the absence of plasma in spark plasma sintering, Scripta Materialia 60 (10) (2009) 835–838.

[20] G. Bernard-Granger, A. Addad, G. Fantozzi, G. Bonnefont, C. Guizard, D. Vernat, Spark plasma sintering of a commercially available granulated zirconia powder: comparison with hot-pressing, Acta Materialia 58 (9) (2010) 3390–3399.

[21] H. Borodianska, T. Ludvinskaya, Y. Sakka, I. Uvarova, O. Vasylkiv, Bulk $Ti_{1-x}Al_xN$ nano-composite via spark plasma sintering of nanostructured $Ti_{1-x}Al_xN$-AlN powders, Scripta Materialia 61 (2009) 1020–1023.

[22] H. Borodianska, L. Krushinskaya, G. Makarenko, Y. Sakka, I. Uvarova, O. Vasylkiv, Si_3N_4–TiN nanocomposite by nitration of $TiSi_2$ and consolidation by HP and SPS, Journal of Nanoscience and Nanotechnology 9 (11) (2009) 6381–6389.

[23] P. Loboda, I. Bogomol, M. Sysoev, G. Kysla, Structure and properties of superhard materials based on pseudo-binary systems of borides produced by zone melting, Journal of Superhard Materials 28 (5) (2006) 28–32 (translation of Rus: Sverkhtverdye Materialy).

[24] I. Gunjishima, T. Akashi, T. Goto, Characterization of directionally solidified B_4C–TiB_2 composites prepared by a floating zone method, Materials Transactions 43 (4) (2002) 712–720.

[25] T.H. Courtney, Mechanical Behaviour of Materials, McGraw-Hill, Columbus, 2000.

[26] P. Loboda, Features of structure formation with zone melting of powder boron-containing refractory materials, Powder Metallurgy and Metal Ceramics 39 (9–10) (2000) 480–486.

[27] K. Niihara, R. Morena, D.P.H. Hasselman, Evaluation of K_{IC} of brittle solids by the indentation method with low crack-to-indent ratios, Journal of Materials Science Letters 1 (1982) 13–16.

[28] P. Dahl, I. Kaus, Z. Zhao, M. Johnsson, M. Nygren, K. Wiik, T. Grande, M.-A. Einarsrud, Densification and properties of zirconia prepared by three different sintering techniques, Ceramics International 33 (8) (2007) 1603–1610.

[29] H. Itoh, K. Sugiura, H. Iwahara, Preparation of TiB_2–B_4C composites by high pressure sintering, Journal of Alloys and Compounds 232 (1996) 186–191.

[30] H.R. Baharvandi, A.M. Hadian, Pressureless sintering of TiB_2–B_4C ceramic matrix composite, Journal of Materials Engineering and Performance 17 (6) (2008) 838–841.

[31] A.A. Shul'zhenko, D.A. Stratiichuk, G.S. Oleinik, N.N. Belyavina, V. Ya Markiv, Formation of polycrystalline boron carbide with elevated fracture toughness, Powder Metallurgy and Metal Ceramics 44 (1–2) (2005) 75–83.

[32] S. Tekeli, Fracture toughness (K_{IC}), hardness, sintering and grain growth behaviour of 8YSCZ/Al_2O_3 composites produced by colloidal processing, Journal of Alloys and Compounds 391 (1–2) (2005) 217–224.

[33] S. Yamada, K. Hirao, Y. Yamauchi, S. Kanzaki, High strength B_4C–TiB_2 composites fabricated by reaction hot-pressing, Journal of the European Ceramic Society 23 (2003) 1123–1130.

[34] Y. Waku, N. Nakagawa, T. Wakamoto, H. Ohtsubo, K. Shimizu, Y. Kohtoku, A ductile ceramic eutectic composite with high strength at 1.873 K, Nature 389 (1997) 49–52.

[35] D.R. Clarke, High-resolution techniques and application to nonoxide ceramics, Journal of American Ceramic Society 52 (1979) 236–246.

[36] J. Echigoya, S. Hayashi, K. Sasaki, H. Suto, Microstructure of directionally solidified MgO–ZrO_2 eutectic, Journal of the Japan Institute of Metals 48 (1984) 430–434.